Interaction of supernova remnants: From the circumstellar medium to the terrestrial laboratory

P. Velarde, D. García-Senz, E. Bravo, F. Ogando, A. Relaño et al.

Citation: Phys. Plasmas 13, 092901 (2006); doi: 10.1063/1.2338281
View online: http://dx.doi.org/10.1063/1.2338281
View Table of Contents: http://pop.aip.org/resource/1/PHPAEN/v13/i9
Published by the American Institute of Physics.

Interaction of supernova remnants: From the circumstellar medium to the terrestrial laboratory

P. Velarde
Instituto de Fusión Nuclear, Universidad Politécnica de Madrid, Madrid, Spain

D. García-Senz and E. Bravo
Departament de Física i Enginyeria Nuclear, Institut d'Estudis Espacials de Catalunya (UPC), Barcelona, Spain

F. Ogando[a)]
Instituto de Fusión Nuclear, Universidad Politécnica de Madrid, Madrid, Spain

A. Relaño
Departament de Física i Enginyeria Nuclear, Institut d'Estudis Espacials de Catalunya (UPC), Barcelona, Spain

C. García and E. Oliva
Instituto de Fusión Nuclear, Universidad Politécnica de Madrid, Madrid, Spain

(Received 6 April 2006; accepted 26 July 2006; published online 14 September 2006)

The evolution of supernova remnants (SNRs) represents a useful and natural laboratory for gasdynamics studies. In this paper the results of several hydrodynamical simulations of the propagation and early phases of interaction of two SNRs embedded in a homogeneous interstellar environment are shown. In particular, the hydrodynamic evolution and collision of twin SNRs during their self-similar stage has been simulated using a two-dimensional Lagrangian hydrocode. In addition, the results of a detailed simulation that attempts to set the adequate conditions to reproduce the same phenomenon through laser ablation of two plastic plugs at the laboratory scale are presented. These results indicate that both large-scale and small-scale simulations display several common features that can be used to design an experiment aimed to validate the hydrodynamical codes. Of particular interest are the structures found around the juncture of the two colliding shells produced by the interaction of the remnants. © *2006 American Institute of Physics*. [DOI: 10.1063/1.2338281]

I. INTRODUCTION

The study of the evolution of supernova remnants (SNRs) has been traditionally an important topic of astrophysics. The physical effects produced by the blast wave born in the explosion can be used as a diagnostic tool to constrain theoretical models of supernovae and to understand the structure of the interstellar medium through which they propagate. In the past years, three fortunate facts have expanded the spectrum of public interested in supernova remnants beyond pure astrophysicists: the explosion of SN1987A in the nearby Large Magellanic Cloud (LMC), the role played by the interaction of a blast wave with the interstellar medium as a basic mechanism to explain gamma-ray bursts afterglows, and finally, the development of techniques based on laser beams to replicate these cosmic events in terrestrial laboratories. Concerning the last point, it must be stressed that a remarkable agreement has been found between laboratory results and numerical simulations of the propagation of self-similar shock waves through a diluted medium.[1,2] Nowadays, laboratory experiments relying on high–power laser facilities are reaching a mature stage where, somehow, a central point is to detect which interesting astrophysical situations might be studied with that technique combined with computer simulations. In the following article we analyze in some detail the relevancy of conducting a laboratory experiment designed to reproduce the collision of two supernova remnants, a subject that is interesting not only for astrophysics but for plasma physics as well.

The interaction of supernova remnants in a spiral galaxy is a relatively frequent phenomenon that affects a considerable fraction of the interstellar gas. The approximate number of supernova remnants in a spiral galaxy can be estimated from the expected rate of supernova explosions, $r_{SN} \sim 0.01 - 0.02$ SN/yr, and from the active lifetime of such objects. This led Smith[3] to the conclusion that up to 30% of the interstellar gas in the arms of a spiral galaxy could have been processed in the past by interacting supernova remnants, including our Solar System. On average, the typical size of a remnant at the time of interaction is ~ 30 pc ($1\ \text{pc} = 3 \times 10^{18}$ cm), when the SNR is well settled in a radiative phase. As it is well known, fluid dynamics dominated by radiation transport processes are not easily reproduced in the laboratory. However, under certain conditions the interaction between the remnants will take place when they still belong to the adiabatic phase. Massive stars are predominantly born inside giant molecular clouds, sizing up to 10^{20} cm and whose mass can reach $10^6\ M_\odot$.[4] These stars are born nearly

[a)]Present address: Energiatieteiden Laboratorio, Helsinki University of Technology, Finland.

simultaneously (for astronomical standards), and their existence is brief; for instance, for a representative mass of $\sim 20\ M_{\odot}$ the lifetime is $\sim 10^7$ yr. Because the size of the cloud is not much larger than that of a typical SNR (for instance, $R_{\mathrm{SNR}} \sim 2 \times 10^{19}$ cm for a remnant of age $t_{\mathrm{SNR}} = 2000$ yr), we can expect that two massive stars born within a time of around 10 000 years will have some chance to develop SNRs that interact during their adiabatic phase. In fact, there have been found several candidates for such collisions in the LMC[5] and in the Milky Way,[6] the most interesting being DEM L316, consisting of two spatially connected shell morphologies with enhanced emission at the juncture between the shells. The estimated radii of these shells are 15 pc and 22 pc. respectively, thus radiative losses are not dominant yet.

The collision of two SNRs is a complex problem that has to be handled with multidimensional hydrodynamics. Two-dimensional numerical simulations performed so far (see, for example, Refs. 7 and 8) suggest that the gasdynamics is complicated because of the formation of reflected shocks at the interaction plane, which may penetrate deep into the remnants. Mixing of material across the interphase and development of tunnels may accelerate the process through which both shells will ultimately balance their pressure before completing the merging. On the other hand, the increase of density and temperature around the interaction region enhances the intensity of its high-energy emission (mainly in the x-ray band), and makes this kind of structure an interesting target for astronomical x-ray observatories as well.[9] On the other hand, we do not expect that the existence of these density and pressure enhanced regions will affect the overall dynamics. In principle the four spots around the interaction plane are short lived events, affecting a low amount of gas, and thus their impact on the dynamics should be very limited. Also their transient character will make it very difficult to detect them. In any case, according to Fig. 3, the most favorable region to see emission would correspond to the reverse-reverse shock collision of SNRs coming from massive progenitors.

The main goal of this paper is to study numerically the early stages of evolution of two SNRs colliding during their adiabatic phase using a two-dimensional smoothed particle hydrodynamics (SPH) code. Our calculations differ from previous numerical studies of collision of two SNRs[10] in that we simulate the collision at an earlier stage in the evolution of the remnants. In addition, we also present a detailed simulation that attempts to set the adequate conditions to reproduce the same phenomenon in a terrestrial laboratory. This time, the calculation was carried out with an adaptive mesh refinement (AMR) hydrocode that includes the physics adequate to handle laser ablation. Previous studies have shown that the evolution of a SNR during its initial self-similar stage can be reproduced in the laboratory through the laser ablation of a plastic plug followed by the impact of the debris on a low-density foam, as given in Ref. 11. A step further in this direction is to generate a couple of laser-induced remnants and let them collide. Laboratory experiments of the interaction between two explosions have already been performed by Velazquez *et al.*,[12] although they were not compared to a specific astrophysical simulation, as it is our aim here. As the morphology of the remnants during the self-similar phase consists of two shocks separated by a contact discontinuity, their interaction gives rise to several shocks and pressure waves and imprints a complex structure to the interaction region. The solutions provided by both codes in this interaction region can be compared to confirm the ability and compatibility of the hydrocodes to handle the interaction of self-similar blast waves. As shown below, the numerical simulation of the proposed laser experiment, carried out with the AMR code, supports the results inferred from the SPH code. By conducting in practice the proposed laboratory experiment, we will be able to make a validation test of the hydrocodes. Then it would be more reliable to simulate the interaction of specific supernova models and make predictions of x-ray and radio emission in order to compare to observations. This would allow, for example, to discern if the putative colliding remnants known as DEM L316 are real or merely a random superposition along the visual of two independent explosions, as the recent work of Williams and Chu[13] suggests.

The organization of the paper is as follows. In Sec. II we describe the main features of the SPH code, and the physics that is included. In this same section we give the results of the simulations of the propagation and further collision of two identical SNRs during their self-similar stage. In Sec. III we explain the main features of the AMR hydrocode used to simulate laser ablation and the formation of two blast waves in laboratory conditions. We include in the same section a discussion of the optimal setting of the proposed experimental device, which serves to set the initial and contour conditions of the AMR calculation, as well as the results of different choices of materials and sizes of the experimental setup. Some final discussion and the conclusions of our work are provided in Sec. IV.

II. PROPAGATION AND COLLISION OF TWO IDENTICAL SNRs

A. Case of Chandrasekhar-mass progenitors

The interaction of two spherical blast waves is an axisymmetric process that must be described by using at least a two-dimensional hydrocode. In this respect, there have been several calculations in the past that have used Eulerian hydrodynamics (see, for instance, Ref. 7 and references therein). Here we report on several results concerning the collision of two remnants carried out by using a Lagrangian SPH code. In this technique the fluid is represented by a sample of mass points (particles) that move according to the laws of conservation of mass, momentum, and energy.[14] The continuous properties of the fluid are computed, at each time step, from the spatial distribution of particles through an interpolating kernel. Even though this Lagrangian technique is very common in many areas of astrophysics it has *never been used* to carry out numerical experiments dealing with SNRs. We have adapted the two-dimensional version of the SPH technique given in Ref. 15 to the problem of the propagation and collision of two SNRs during their adiabatic phase. The SPH technique has the advantages of a multidimensional

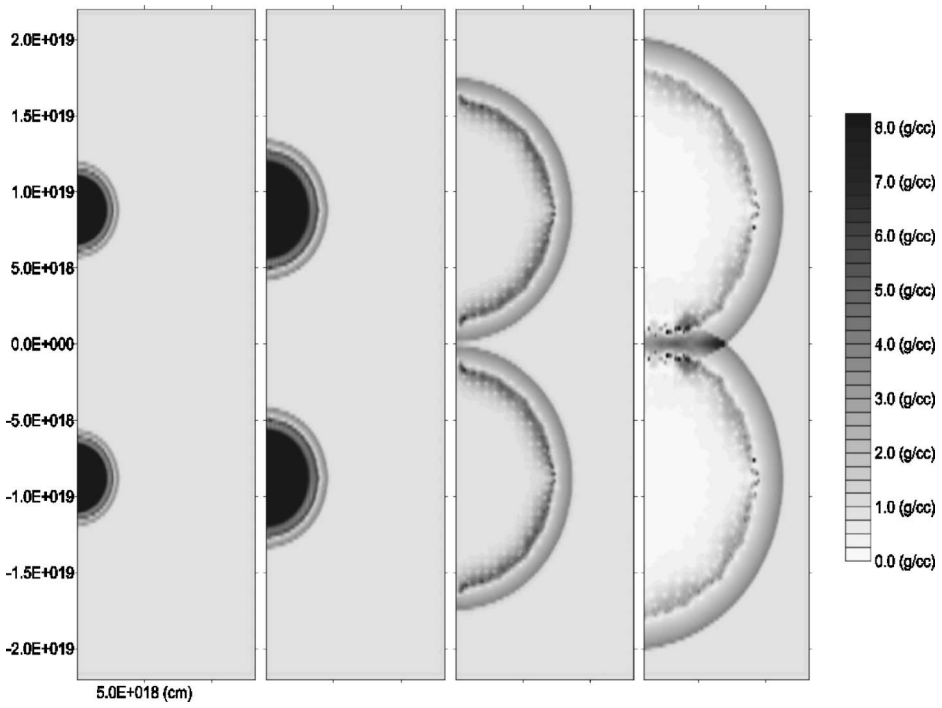

FIG. 1. Snapshots of the density evolution (in 10^{-24} units) of two identical SNRs originated from a type Ia-like explosion (progenitor mass 1.4 $M_{\odot}$) at times $t=33$ yr, $t=80$ yr, $t=266$ yr, and $t=431$ yr, respectively. Here the axis of symmetry (z axis) is the vertical line. Collision takes place at $z=0$ pc and $t\simeq 280$ yr, a little after the third picture. In the last snapshot we can see the four high-density spots arising from the successive interactions of forward and reverse shocks. There are approximately 1400 particles in the forward-forward spot, around 230 particles in the reverse-reverse, and only 14 in each spot arising from off-axis forward-reverse collision. Therefore while in the two former cases the interaction is well represented, in the last case the emerging features were probably strongly smoothed by the interpolation procedure.

Lagrangian code and, in particular, is ideally suited for problems that cover a large range of spatial scales but that focus the mass in one place, as in the collision of two remnants. It also avoids any numerical diffusion, and conserves both angular momentum and linear momentum by construction. For a long-term project such as ours, in which we would like to finally apply the same code to predict the x-ray emission from two interacting remnants and compare the results with observations of DEM-L316, the Lagrangian nature of SPH allows us to follow the nonequilibrium ionization of shocked matter and later compute its emission properties (map, flux, spectra). Our interest here is then to validate the code in a scenario as close as possible to the conditions in which it will be applied to the collision of remnants in a general case.

Our initial model consists of a sample of 208 000 particles settled in a rectangular grid defined in the plane (r,z) of cylindrical coordinates. This region, sizing 4.3 pc $\times 14.25$ pc, is large enough to follow the evolution of the two remnants from the initial energy deposition until their ultimate collision. Self-gravity does not play a significant role in the dynamics and was neglected. Pressure was computed directly from the specific internal energy, u, assuming an ideal gas equation of state, $P=(\gamma-1)\rho u$, with $\gamma=5/3$, and the energy equation contained no heat term, so an adiabatic evolution was assumed, which is reasonable for remnants aging less than $\sim(2-3)\times 10^4$ yr. Shock waves were handled by using a standard artificial viscosity scheme. The mass of the particles was conveniently arranged in order to reproduce the initial density profile of the system, which was taken to follow a power law with a central plateau (see Fig. 2), as usual for SNR studies:

$$\rho(t=0)=\begin{cases}\rho_1 & r<r_1\\ \rho_1(r/r_1)^{-n}, & r_1<r<r_2\\ \rho_2 & r>r_2.\end{cases} \quad (1)$$

In the above expressions we choose $n=7$, as appropriate for type Ia supernovae, and the rest of parameters are as follows: $\rho_1=1.76\times 10^{-21}$ g/cm^3, $r_1=0.2$ pc and $r_2=0.58$ pc, and $\rho_2=10^{-24}$ g/cm^3, which is the standard value for the dilute interstellar medium. Such a value, $n=7$, is usual in SNR studies because many one-dimensional hydrodynamical simulations have shown that the density profile can be reasonably fitted through a central plateau followed by a power-law distribution with $n\simeq 7$ (for type Ia supernovae) and $n\simeq 12$ (type II).

Because of the large integration domain, the number of particles belonging to each ejecta was low, $N_{\mathrm{SN}}=1726$. Among them the larger number, 1530, reside in the power-law part of the ejecta while only 196 belong to the central plateau. We think that 1530 particles are sufficient to handle the outstanding features of the self-similar stage before the collision (see below). The explosion was initiated by depositing 10^{51} ergs of kinetic energy inside the sphere of radius r_2. Such kinetic energy was radially distributed, matching a homologously expanding profile, $v=v_{\max}(r/r_2)$, with $v_{\max}=23\,480$ km/s. Both twin explosions were triggered at symmetrical centers $z=\pm 2.85$ pc, so that they should meet around the line defined by $z=0$ pc.

The evolution of the remnants is depicted in Figs. 1 and 2. After a transit period lasting $t\sim 30$ yr, and until the onset of the interaction between both remnants, the evolution becomes self-similar, as can be seen in Fig. 2. From that time on the structure of each SNR consists of a blast wave (or forward shock) coupled through a contact discontinuity to a reverse shock that propagates into the ejecta. The evolution during the self-similar period can be compared to analytical solutions, providing an initial check of the correctness of the simulation. In our calculations, the ratio between the peak density of the reverse and forward shocks at $t=80$ yr was

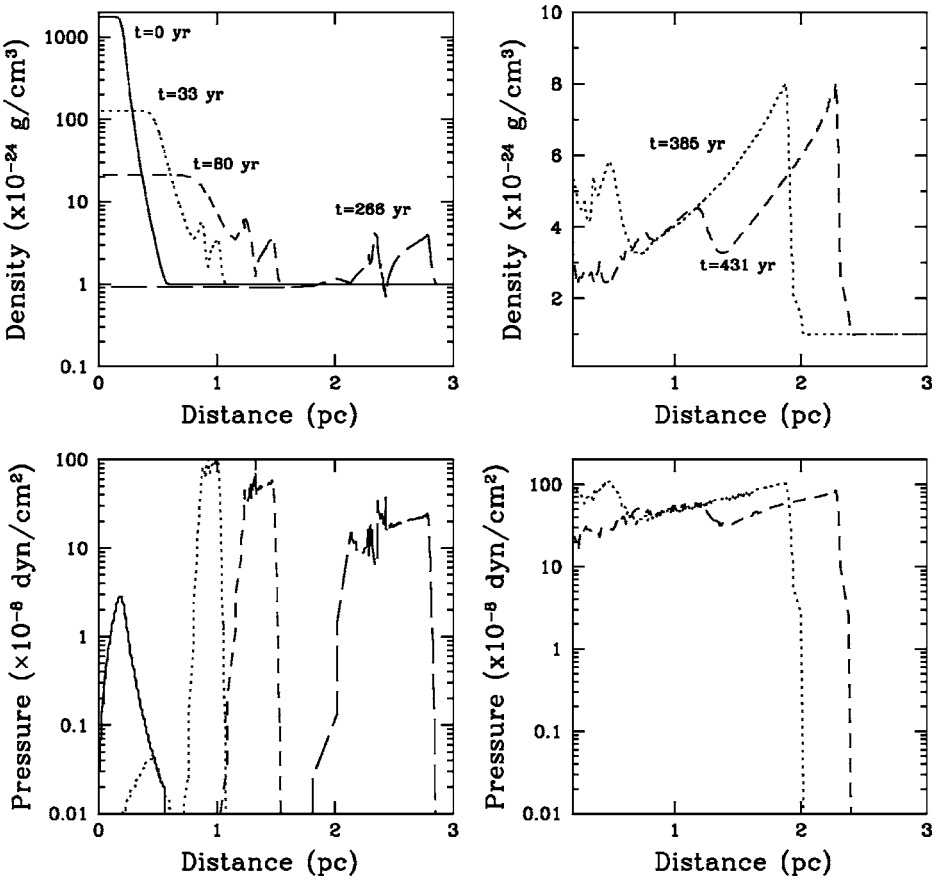

FIG. 2. Density and pressure profiles during the adiabatic evolution of the remnants (case of Chandrasekhar-mass progenitors), corresponding to a cut around the line $z=2.85$ pc (left), which passes through the explosion center of one of the remnants, and to the collision line, $z=0$ pc (right), respectively. As we can see, the evolution remains self-similar at the displayed times, although at $t=266$ yr the reverse shock has already become weaker. The spikes in pressure are purely numerical due to the use of the artificial viscosity scheme to handle shock waves in the SPH code. On the collision line (right) both density and pressure profiles display the effects of the interaction between the remnants.

$\rho_{rs}/\rho_{fs}\sim 1.65$, higher than that predicted analytically ($\rho_{rs}/\rho_{fs}=1.3$, see Ref. 16) owing to the limited number of particles used to represent the supernova matter and to the strong sensitivity against the density profile adopted for the ejecta [exponent n in Eq. (1)]. A relevant parameter in this period is the so-called Euler number defined as $\mathrm{Eu}=v\sqrt{\rho/P}$, where v, ρ, and P must be taken from a representative structure of the system. It has been shown[17] that two physical systems described by the Euler equations, but with different length scales, are related by a simple scale transformation if they share the same Euler number. Here we took the distance between the forward and the reverse shocks to set the scale ratio between the SNR evolution and the terrestrial laboratory simulations reported below. In fact, the strong shock conditions for the forward shock in combination with the self-similar solutions (see Table 1 in Ref. 16) lead to a definite value of the Euler number in each region. For $\gamma=5/3$ it gives $\mathrm{Eu}_{rs}=3.6$. Taking the values of ρ, P, and v, in the densest region of the reverse shock from the numerical model we inferred $\mathrm{Eu}_{rs}=3.66$ at $t=80$ yr, in good agreement with the above analytical estimation.

At $t\sim 280$ yr the collision between the two remnants around the line $z=0$ pc starts. As the colliding self-similar waves have some degree of internal structure, the interaction is richer than a simple collision of strong shocks. The interaction between the incoming forward shocks leads to the formation of a high-pressure region around the juncture of the shells, which propagates outward (last snapshot of Fig. 1) along the $z=0$ pc line. As a consequence, there is a new increase of density and pressure in a small region near the separation plane with respect to their steady values by factors ~ 2 and ~ 5.8, respectively (see Fig. 3, solid line). Thus, one can expect an increase in the ionic temperature of a factor $P/\rho\sim 2.9$ near the symmetry axis. The high-pressure spot moves through the line defined by $z=0$ pc, sending pressure waves toward the interior of the double-shocked region. The successive reflections of these pressure waves on the contact discontinuity and on the other traveling shock waves leads to a complicated pattern of pressure and density distribution in the double-shocked volume (this volume is, in fact, a torus because of the cylindrical symmetry of the calculation). A secondary peak can also be seen in Figs. 2 and 3. This secondary maximum corresponds to the time the reverse shocks meet. On the whole we would expect to see four high-pressure and high-density regions associated to the forward-forward, reverse-reverse, and forward-reverse shocks, respectively, the two former just on the collision line and the pair of forward-reverse spots symmetrically located around that line. As we can see, all these features are present in the last snapshot of Fig. 1. A comparison between a laboratory experiment of colliding SNR with a hydrodynamical simulation, similar to that given in this section, should take advantage of the intensity and location of these spots to validate the numerical scheme. We will bring more elements to make such a comparison in Sec. III through the simulation of the laboratory experiment using an AMR hydrocode.

A complication not mentioned above is the role played by instabilities during the SNR self-similar stage. In particu-

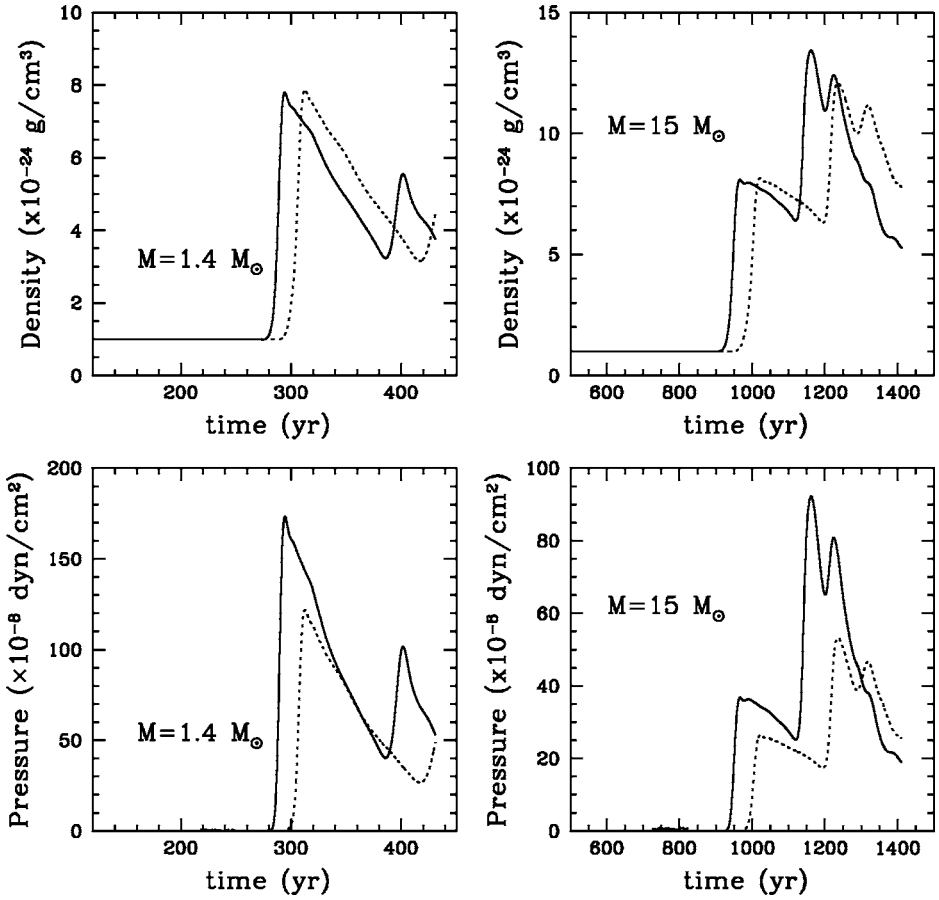

FIG. 3. Time evolution of density and pressure of two selected particles located at the collision plane for the Chandrasekhar-mass progenitors case (left) and the massive progenitors case (right). The initial (r,z) coordinates of these particles are (0.66,0) pc (solid line) and (1.0,0) pc (dotted line) in the first case, and (0.90,0) pc (solid line) and (1.38,0) pc (dotted line) in the second one. The origin of the split of the higher peak in the 15 $M_\odot$ is due to the convergence of the waves launched during the off-axis forward-reverse shock collision. Because of the high degree of symmetry of our system, these shock waves meet simultaneously at the $Z=0$ pc axis, leading to a new increase of pressure and density shortly after the reverse-reverse shock interaction has previously set the absolute peaks of these variables.

lar, it is well known that the region located between the contact discontinuity and the reverse shock is prone to the Rayleigh-Taylor instability. However, we have chosen not to include that effect in our current simulations (i.e., no perturbation was seeded at the beginning of the self-similar phase) because it may blur the four spots features after the collision of the remnants making the diagnosing harder. On the other hand, the simulations with ARWEN did not show any indication of Rayleigh-Taylor instability growth during the simulation.

B. Case of massive progenitors

We consider now a pair of 15 $M_\odot$ stars as progenitors of twin SNRs and set them at a distance such that their interaction begins $\sim$860 yr after the explosion. In this simulation, we used 208 000 particles located in a rectangular grid of 6 pc$\times$20 pc. Equation (1) was used again to generate the initial density profile, this time with $n=12$, $\rho_1=4.25\times10^{-22}$ g/cm^3, $\rho_2=10^{-24}$ g/cm^3, $r_1=0.71$ pc, and $r_2=1.22$ pc. The number of particles representing each ejecta was $N_{SN}=4484$, higher than in the previous case owing to the larger domain encompassed by the SNRs. The explosion was initiated by depositing 10^{51} ergs of kinetic energy inside the volume defined by r_2. As in the previous case, the kinetic energy was radially distributed matching a homologous velocity profile, $v=v_{max}(r/r_2)$, with $v_{max}=4900$ km/s. The center of the explosions was at $z=\pm4$ pc, so that they meet around the line defined by $z=0$ pc.

The evolution of the remnants is depicted in Fig. 4. After a period lasting roughly $t\sim500$ yr, the evolution becomes self-similar. Afterward a blast wave coupled to a reverse shock through a contact discontinuity is formed. The ratio between the density peak of the forward and reverse shocks at $t=671$ yr is $\rho_{rs}/\rho_{fs}=5.75$, much higher than in the previous case but still lower than that predicted analytically ($\rho_{rs}/\rho_{fs}=7.2$, Ref. 16). As in the case of 1.4 $M_\odot$ progenitors, the discrepancy may be attributed to the strong sensitivity of the SNRs dynamics against the particular density profile adopted for the ejecta [even more severe now because the higher value of the exponent n in Eq. (1)]. Probably for the same reason we found a Euler number, $Eu_{rs}=5.8$ at $t=671$ yr, which is below the analytical estimation $Eu_{rs}=7.5$ (inferred from Table 1 in Ref. 16).

At $t=860$ yr the collision between both remnants around the line $z=0$ pc starts. Although the interaction follows a similar trend as in the previous case there are also significative differences. In particular, the higher values of pressure and density in the reverse shocks lead to a much more pronounced secondary peaks following the collision as can be seen in Figs. 3 and 4. Therefore, for type II supernovae both pressure and density reach their absolute maximum not during the forward-forward shock interaction but because of the reverse-reverse shock collision.

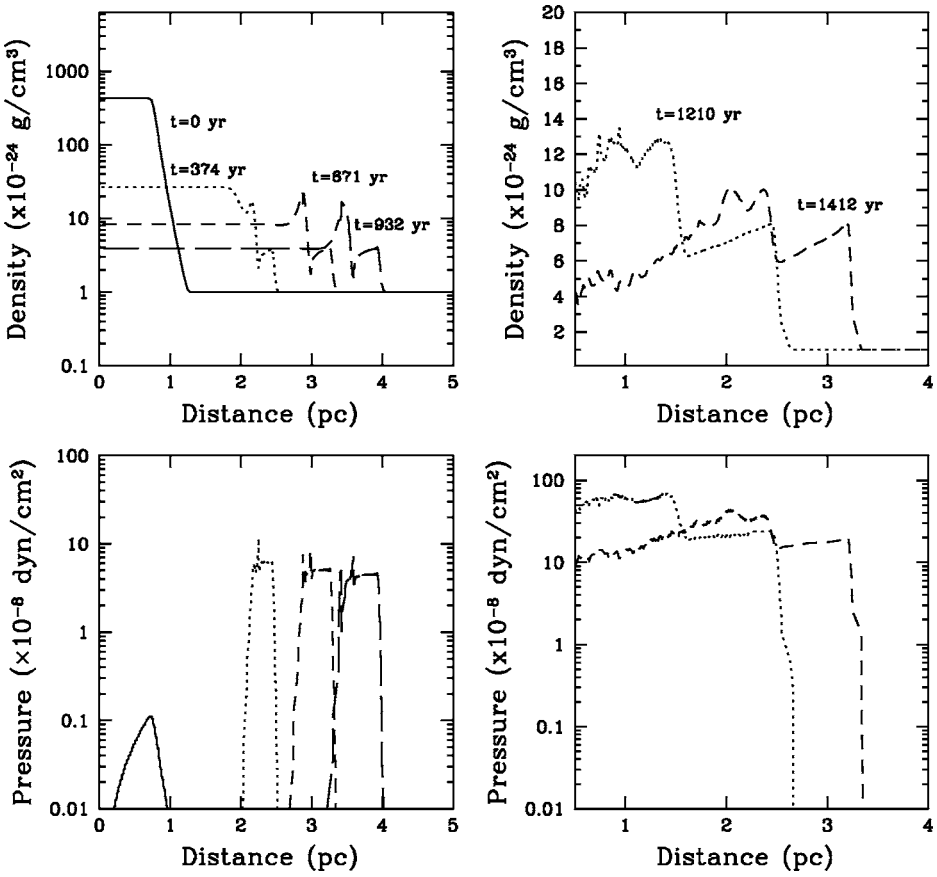

FIG. 4. Density and pressure profiles during the adiabatic evolution of the remnants (case of massive progenitors), corresponding to a cut around the $z=4$ pc (left) and to the collision line, $z=0$ pc (right), respectively.

III. SCALING OF THE ASTROPHYSICAL SIMULATION TO THE TERRESTRIAL LABORATORY

A. The ARWEN (Ref. 18) code

The simulations of blast wave interactions at the laboratory scale were carried out with the hydrocode ARWEN. All the calculations were performed in two-dimensional cylindrical geometry (see Figs. 5 and 7), being the actual calculated region one half of the physical system. There is a plane along which the collision takes place at the upper boundary in the simulations. The main geometrical features are shown in Fig. 5; the main device is a cylinder with a diameter of 2200 μm and a length of 3000 μm along the axis. As materials of the targets we have considered CH and Si, which also gave satisfactory results in Drake *et al.*'s[11] experiments of single remnants. Although we have considered direct and indirect laser illumination, the simulations below were calculated using direct illumination with a spot size of 100 μm so that it induced a curved, although not spherical, blast wave traveling through the foam. The ARWEN code was designed to perform calculations of high-temperature and high-density fluids. These thermodynamic conditions are commonly reached in laser-produced plasmas, with laser intensities over 10^{10} W/cm^2. These kinds of plasmas are obtained in laser-driven experiments, as the one proposed in this article. The equation of state is the quotidian equation of state (QEOS) fitted to experimental Hugoniot data via a pressure multiplier. In the actual calculations shown in the figures and discussed in more detail in the text, laser energy is deposited along the parallel rays via an inverse bremsstrahlung, with the rest of the energy deposited directly in the turning point.

The code ARWEN solves numerically the compressible fluid dynamics equations with electron heat conduction and radiation transport. We separate these three main calculations by operator splitting. The computational fluid dynamics (CFD) operator part is a Godunov-type scheme, with the Riemann problem solved in one or two temperatures (electronic and ionic) and with linear or parabolic reconstruction of the profiles.[19,20] Electron heat conduction is incorporated using a multigrid technique with parabolic interpolation at the boundaries. Since heat conduction coefficients are flux limited, special care must be taken to handle properly the nonlinear behavior of the solution. For instance, convergence can be achieved very slowly. In this case, switching among different methods is used to improve the performance of the code. Data from accurate equations of state (EOS) and opacities are crucial for realistic simulations since the ideal gas model is no longer valid in the treated thermodynamic ranges. ARWEN uses EOS data from tabular databases especially designed for fast access. Data may be imported from different sources such as SESAME or the analytical model QEOS.[21] Opacities are imported from the Jimena[22] code.

The accurate treatment of radiation transport and interaction with matter is essential in the simulation of the laboratory experiment. The radiation calculations are performed with the discrete ordinate scheme (S_N), which allows to know the propagation direction. The calculated radiation

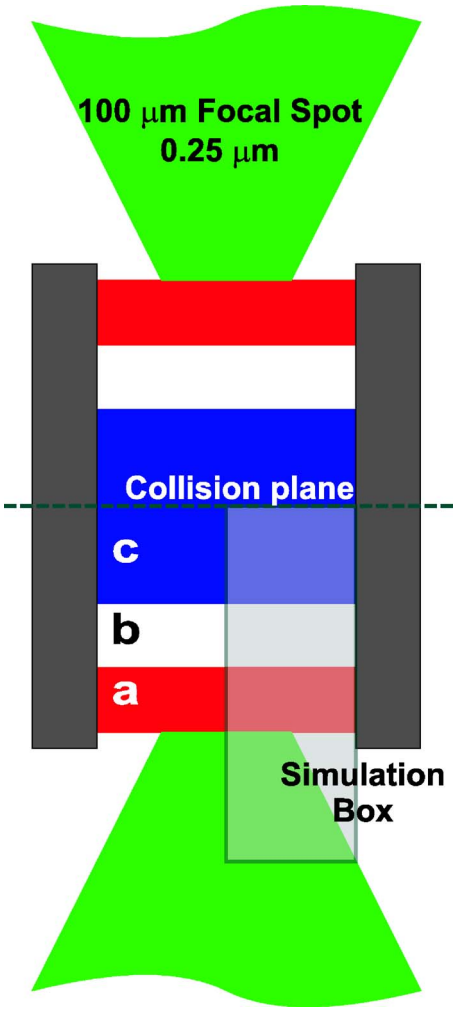

FIG. 5. Proposal of a target for analyzing the collision between SNRs. In this figure material "a" is the plastic plug made of CH, "b" is the vacuum gap, and "c" represents the foam.

field is coupled to the fluid dynamics, i.e., absorption and emission processes are taken into account in the calculations. The implementation of the interaction of radiation with matter results in an emission term dependent on the radiation intensity itself. It has to be stressed that conventional algorithms show an important problem for achieving convergence in that case, which can be solved introducing sophisticated acceleration techniques. The method of diffusion synthetic acceleration (DSA, see Ref. 23) has been implemented in our calculations to overcome those difficulties.

All the calculations presented here have been performed under the block structured adaptive mesh refinement (BS-AMR) environment for optimum performance. The algorithms concerning BS-AMR involve both the resolution of multiple single-mesh calculations on homogeneous orthogonal meshes, and the exchange of data between the obtained results. Meshes are organized in hierarchical sets, each with the same cell size. This exchange of data, as commonly done in CFD,[24] implies transmission of inward boundary conditions from coarse levels to finer ones, and correction of the coarse solutions by means of the finer ones. All the data handling specific from AMR has been treated using the BoxLib library programmed in C++. The library allows for a parallel run in the code due to its internal structure,[25] simplifying parallelization tasks to the programmer.

Due to the nonlinear dependence of emission with density and temperature, even under local thermodynamic equilibrium (LTE), a special key point of the transport of thermal radiation lies in the proper calculation of radiation emission. The emissivity of regions with steep gradients of density and/or temperature has to be calculated to try to reproduce the real profiles from the discrete data. Otherwise, the obtained values using different cell sizes (as is usual in AMR) may be inconsistent, resulting in the need for strong corrections among levels and degradation of the convergence rate.

Finally a few words concerning to the capabilities of ARWEN to resolve the four density spots and other detailed structures: ARWEN is a block adaptive mesh code, thus patches of increasing resolution are placed where needed, according to a comparison of gradients of several magnitudes. It means that the code can track the fine structure of the flow. Boundary conditions for fluid motion are free flow (bottom and right) and wall type (top and left).

B. Proposed experimental setup

The design of the target is similar to that used by Drake *et al.*,[11] and we obtain similar results for the remnant evolution prior to collision. As mentioned before, the main difference lays on the EOS because we use QEOS. A cartoon of the proposed experimental device is shown in Fig. 5, which basically consists of two plastic plugs with $\rho=1044$ kg/m^3, located at the two sides of the box separated by a vacuum gap of 150 μm from a low-density foam ($\rho_{\text{foam}}=45$ kg/m^3) placed at the center of the box. The goal of the vacuum gap is to make easier the emergence of an homologous profile for the debris ejected after the evaporation of the two plastic plugs. The low-density foam is the laboratory equivalent of the interstellar medium. Its width, $\Delta l_{\text{foam}}=2200$ μm, density, and composition (SiO_2) were chosen to ideally match the conditions prevailing in cosmic SNR after scaling. A potential difficulty could arise because the preheating and melting of the target due to the low-density tail of the plug. In this respect, Ref. 11 already considered the effect of radiation emitted by the shocked foam into the dynamically unperturbed part. They concluded that, for their experimental setup, there was a minimum foam density in order that radiation would not have dynamical consequences. Such a density was determined as 20 mg cm^{-3} lower than that proposed in our experiment, $\rho_{\text{foam}}=45$ mg cm^{-3}.

Concerning the diagnostic technique, the pioneering experiments performed by Ref. 11 were diagnosed through x-ray backlighting with the aid of a streak camera. More modern techniques involves the use of a backlight x-ray plus Bragg crystals,[26,27] giving a resolution of about 10–20 μm. Another interesting technique is tunable diode laser absorption, which might allow simultaneous measurement of the

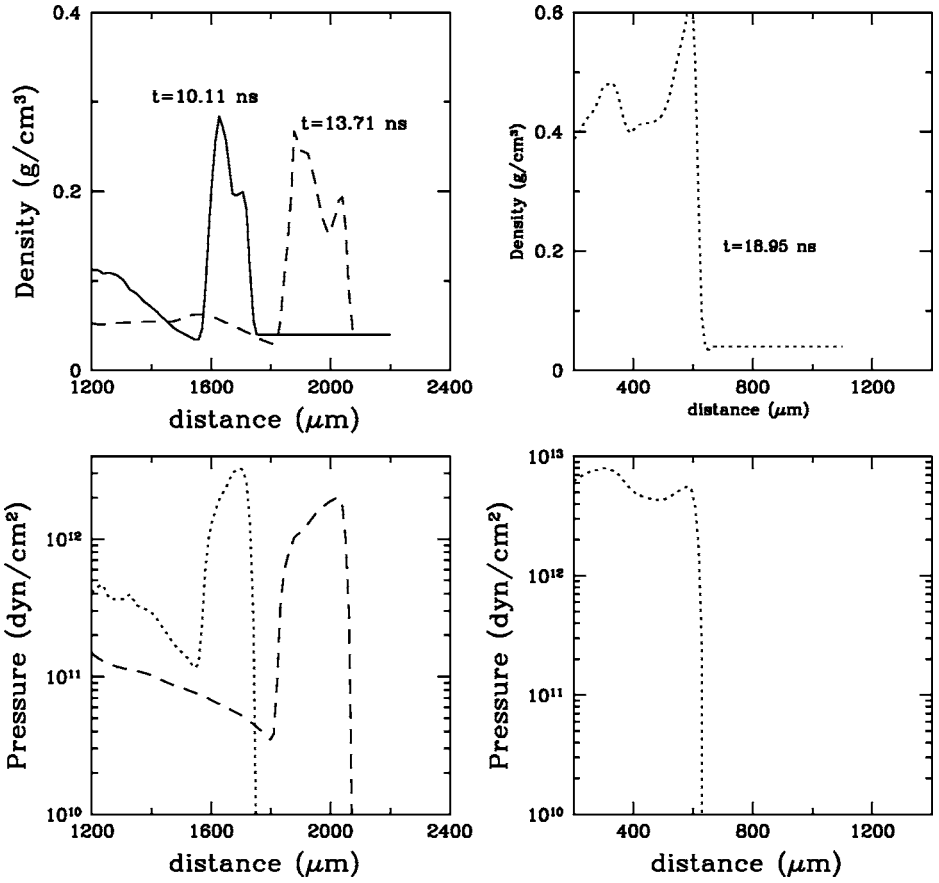

FIG. 6. Density and pressure profiles during the evolution of a target simulated with ARWEN (compare to Fig. 2 belonging to the astrophysical case).

heavy ion temperature and density on a CCD. At the present stage of development of our project, we have not yet determined which is the optimal experiment diagnostic technique.

C. Simulation of the collision in laboratory conditions

We have run cases both with a direct and indirect drive, with laser pulses from 15 J to 10 kJ (and their equivalents in radiation temperature) and using SiO_2 and CH targets and found that the 8 kJ and 3 kJ cases provided a good comparison to the above described simulations of SNRs. In Fig. 6 we show several one-dimensional profiles of density and pressure at different times. In particular, the left panel of Fig. 6 displays the evolution before the collision of the remnants. At first glance there is a qualitative similitude with Fig. 2, belonging to SNRs, and we can see the typical double shock structure. A more quantitative comparison is possible as long as the Euler number, Eu, of both calculations is similar. From the laboratory simulation we get $\mathrm{Eu}\simeq 3.5$ (at $t=10.11$ ns) and $\mathrm{Eu}\simeq 3.7$ (at $t=13.71$ ns), which agrees with the characteristic Euler number of low-mass explosion progenitors ($\mathrm{Eu}\simeq 3.6-3.7$, see Sec. II A) in the cosmic case but not with the case of massive progenitors ($\mathrm{Eu}\geq 5.5$, Sec. II B). We interpret these results as meaning that the (approximately) homologous density profile of the ablated plastic is closer to Eq. (1) with $n=7$ than with $n=12$. Therefore, there is a direct equivalence between the results of Sec. II A and the proposed laboratory experiment. It is surprising that the astrophysical case, calculated using SPH, besides being really basic physics, and its terrestrial analog calculated through an AMR code that incorporates a complex physics, keeps such a degree of similarity. The reason is that, according to Kane *et al.*,[17] the hydrodynamical evolution following any initial rapid energy deposition has a weak dependence on the particular EOS and against radiative transport effects. However, transport processes have to be included to describe the laser-matter interaction in the target. On the other hand, the analysis of the evolution of the Euler number in both scenarios does not show any significant divergence at the time the collision takes place. Hence the comparison is meaningful. Taking the distance between the forward and the reverse shock as a characteristic length scale, it is possible to find the adequate scale relationships linking both phenomena.[17] In our numerical experiments a correspondence is found between the structure of SNR at $t\simeq 80$ yr and that of the laboratory microtarget at $t=10.11$ ns: $100\ \mu\mathrm{m(lab)}\simeq 0.38$ pc (SNR) and 1 ns(lab) $\simeq 33$ yr (SNR). Such a temporal equivalence 1 ns/33 yr can be now used to find the optimal thickness of the foam layer in the proposed terrestrial experiment (see Fig. 5). In the simulation given in Sec. II A, the interaction between SNRs born from type Ia supernovae explosions approximately starts at 280 yr. Therefore the equivalent laboratory time is $t_{\mathrm{lab}}^{\mathrm{col}}\simeq(280-80)\ \mathrm{yr}\times 1\ \mathrm{ns}/33\ \mathrm{yr}+10.11\ \mathrm{ns}=16.2$ ns. After running several simulations we have found that $\Delta l_{\mathrm{foam}}=2200\ \mu$m led to that interaction time. A snapshot of the density and pressure distribution inside the experimental device once the collision is fully developed at t=19.2 ns is shown in Fig. 7. A comparison of the density

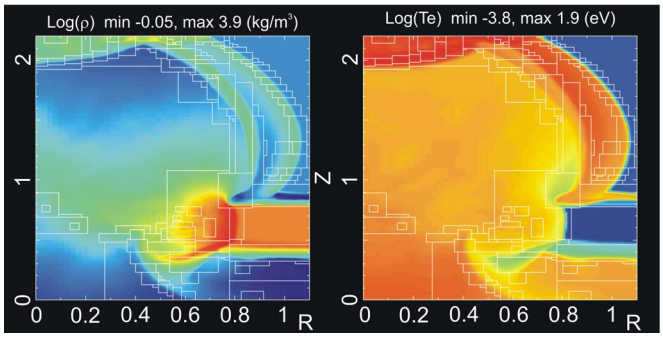

FIG. 7. Density (left) and temperature (right) plots in logarithmic scale after collision ($t=19.2$ ns). The units of the axis are given in millimeters. The line of interaction is $Z=2.2$ mm and the axisymmetrical z axis is the vertical ones. We can distinguish the curved forward and reverse shocks separated by a darker zone (the contact discontinuity) at the upper-right region of the plot. The collision is going on in the upper-left part of the picture, sliding to the right as time progresses, through the $Z=2.2$ mm line.

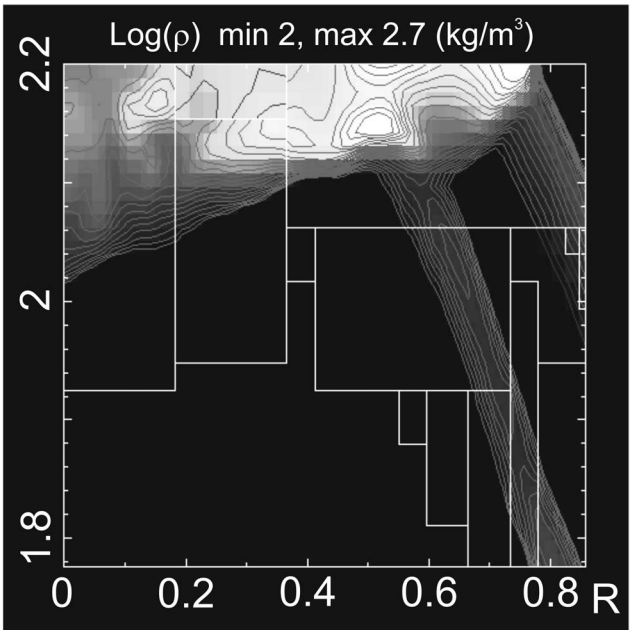

FIG. 8. Density contours in the collision region at $t=20.9$ ns, showing the structure of the interactions between the different shock waves. The units of the axis are given in mm. This image is the laboratory counterpart of the last image (lower semiplane) shown in Fig. 1 corresponding to the astrophysical case at the equivalent time $t=431$ yr. Note that as in the previous figure the forward and reverse shocks separated by a darker gap are visible at the right part of the plot. The forward-forward spot just at the upper-right corner is the most visible feature. However, half of the reverse-reverse interaction region is also apparent at coordinates (0.5,2.2) mm, as well as one of the forward-reverse spots at (0.5,2.15) mm (the other spot lies above $Z=2.2$ mm owing to the reflective boundary conditions).

and pressure profiles on the collision line, at equivalent times between cosmic and laboratory SNRs, can be done by inspection of Figs. 2 and 6 (the three profiles shown in Fig. 6 correspond to times 80, 266, and 385 yrs in Fig. 2). As we can see, the morphology of the profiles in both calculations is very similar. There is a big jump in density associated to the collision of the forward shocks as well as a secondary maximum close to the z axis. The pressure profiles are also in qualitative agreement. There are, however, some quantitative differences worthy of mention. The density jumps on the laboratory simulation (with respect the initial foam density) are about 50% higher than in their astrophysical counterpart. These differences probably arise because of the very different EOS used in both simulations. Quantitative differences in the relative distances between the principal and secondary peaks are due to the different curvatures of the shocks in both simulations. In Fig. 8 there is a zoom of the neighborhoods of the collision region at $t=20.9$ ns. The high-density spots associated to the forward-forward and forward-reverse shocks are clearly visible. The reverse-reverse shock interaction is less pronounced but also visible at the similar distance from the z axis than the forward-reverse spot. On the whole such geometry matches well with that shown in the last snapshot shown in Fig. 1 concerning the astrophysical scenario at the equivalent time $t=431$ yr. In that figure the four density spots are quite well marked, although, again, the reverse-reverse shock interaction is less intense. Moreover, it is located closer to the z axis than in the laboratory experiment owing to the higher curvature of the front.

IV. CONCLUSION

In this paper we have studied a particularly demanding problem consisting of the interaction of twin SNRs. These objects owe a doubly shocked structure connected by a contact discontinuity, thus its interaction contains more of a substructure than that of a single shock waves. We have performed two-dimensional simulations of the interaction, devised an experimental setup intended to reproduce the phenomenon at laboratory scales, and tested the latter by accurate numerical simulation with an AMR code.

The codes used in the simulations were quite different: a Lagrangian SPH code was used for solving the astrophysical problem, while a Godunov-type Eulerian scheme was at the base of the ARWEN code. The physics included was also adapted in each case to the particular problem. For instance, the EOS used in the SPH calculations was that of an ideal gas, while the ARWEN code incorporates realistic EOS for solid targets, among others. The evolution and collision of SNRs was computed assuming adiabaticity in the SPH code, yet the ARWEN code includes radiation transport modules, necessary in order to predict and analyze the plates that will be obtained in a laboratory experiment.

Both codes solved the corresponding problems with success and the results compare well with each other. Particularly interesting were the substructures that developed in the zone affected by the interaction of the twin blast waves. If detected experimentally, these structures could provide a means to validate the adequacy of the codes to the simulations.

By solving this demanding problem, we have established the basis for attacking more complex situations and even for trying to modelize and replicate in the laboratory real SNRs like, for instance, the interacting remnants known as DEM L316 in the Large Magellanic Cloud. Our next step will be to perform the proposed experiment.

ACKNOWLEDGMENTS

The authors thank the anonymous referee for his many suggestions that have improved the general presentation of the text, and acknowledge the financial support given by the MCyT within the programs AYA2002-04094-C03 and ENE2005-02064/FTN.

[1] J. Kane, R. P. Drake, and B. A. Remington, Astrophys. J. **511**, 335 (1999).
[2] K. Keilty, E. Liang, B. Remington, R. London, K. Estabrook, and J. Kane, Astrophys. J., Suppl. Ser. **127**, 375 (2000).
[3] B. W. Smith, Astrophys. J. **211**, 404 (1977).
[4] F. H. Shu, F. C. Adams, and S. Lizano, Annu. Rev. Astron. Astrophys. **25**, 23 (1987).
[5] R. M. Williams, Y. H. Chu, J. R. Dickel, R. Beyer, R. Petre, R. C. Smith, and D. K. Milne, Astrophys. J. **480**, 618 (1997).
[6] B. Uyaniker, W. Reich, A. Yar, R. Kothes, and E. Frst, Astron. Astrophys. **389**, L61 (2002).
[7] M. Rozyczka, G. Tenorio-Tagle, and P. Bodenheimer, Astron. Astrophys. **167**, 120 (1986).
[8] S. Yoshioka and S. Ikeuchi, Astrophys. J. **360**, 352 (1990).
[9] M. Nishiuchi, J. Yokogawa, K. Koyama, and J. P. Hughes, Publ. Astron. Soc. Jpn. **53**, 99 (2001).
[10] P. Bodenheimer, H. W. Yorke, and G. Tenorio-Tagle, Astron. Astrophys. **138**, 215 (1984).
[11] R. P. Drake, T. B. Smith, J. J. Carroll III, Y. Yan, S. G. Glendinning, K. Estabrook, D. Ryutov, B. A. Remington, R. J. Wallace, and R. McCray, Astrophys. J., Suppl. Ser. **127**, 305 (2000).
[12] P. F. Velázquez, H. Sobral, A. C. Raga, M. Villagrán-Muniz, and R. Navarro-González, Rev. Mex. Astron. Astrofis. **37**, 87 (2001).
[13] R. M. Williams and Y. H. Chu, Astrophys. J. **635**, 1077 (2005).
[14] J. J. Monaghan, Annu. Rev. Astron. Astrophys. **30**, 543 (1992).
[15] L. Brookshaw, ANZIAM J. **44**, C114 (2003).
[16] R. Chevalier, Astrophys. J. **258**, 790 (1982).
[17] D. Ryutov, R. P. Drake, J. Kane, E. Liang, B. A. Remington, and W. M. Wood-Vasey, Astrophys. J. **518**, 821 (1999).
[18] F. Ogando and P. Velarde, J. Quant. Spectrosc. Radiat. Transf. **71**, 541 (2001).
[19] P. Colella, J. B. Bell, and J. Trangenstein, J. Comput. Phys. **82**, 362 (1989).
[20] G. H. Miller and E. G. Puckett, J. Comput. Phys. **128**, 134 (1996).
[21] R. M. More, K. H. Warren, D. A. Young, and G. B. Zimmerman, Phys. Fluids **31**, 3059 (1988).
[22] E. Mínguez, J. F. Serrano, and M. L. Gámez, Laser Part. Beams **6**, 265 (1998).
[23] R. E. Alcouffe, B. A. Clark, and E. W. Larsen, *Multiple Time Scales* (Academic, Orlando, 1985), p. 73.
[24] M. J. Berger and J. Oliger, J. Comput. Phys. **53**, 484 (1984).
[25] C. A. Rendleman, V. E. Beckner, M. Lijewski, W. Y. Crutchfield, and J. B. Bell, Computing and Visualization in Science **3** (2000).
[26] D. B. Sinars, G. R. Bennet, D. F. Wenger *et al.*, Rev. Sci. Instrum. **75**, 3672 (2004).
[27] D. B. Sinars, M. E. Cuneo, B. Jones *et al.*, Phys. Plasmas **12**, 56305 (2005).